Variability v.s. synchronicity of neuronal activity in local cortical network models with different wiring topologies

Katsunori Kitano · Tomoki Fukai

Abstract Dynamical behavior of a biological neuronal network depends significantly on the spatial pattern of synaptic connections among neurons. While neuronal network dynamics has extensively been studied with simple wiring patterns, such as all-to-all or random synaptic connections, not much is known about the activity of networks with more complicated wiring topologies. Here, we examined how different wiring topologies may influence the response properties of neuronal networks, paying attention to irregular spike firing, which is known as a characteristic of *in vivo* cortical neurons, and spike synchronicity. We constructed a recurrent network model of realistic neurons and systematically rewired the recurrent synapses to change the network topology, from a localized regular and a "small-world" network topology to a distributed random network topology. Regular and small-world wiring patterns greatly increased the irregularity or the coefficient of variation (Cv) of output spike trains, whereas such an increase was small in random connectivity patterns. For given strength of recurrent synapses, the firing irregularity exhibited monotonous decreases from the regular to the random network topology. By contrast, the spike coherence between an arbitrary neuron pair exhibited a non-monotonous dependence on the topological wiring pattern. More precisely, the wiring pattern to maximize the spike coherence varied with the strength of recurrent synapses. In a certain range of the synaptic strength, the spike coherence was maximal in the small-world network topology, and the long-range connections introduced in this wiring changed the dependence of spike synchrony on the synaptic strength moderately. However, the effects of this network topology were not really special in other properties of network activity.

Keywords Computational model · Neuronal wiring · Small-world network · Synchrony · Irregular firing

1 Introduction

The spatial or topological pattern of neuronal wiring determines how neurons communicate with one another and may be important for information processing performed by neuronal networks (Buzsaki et al. 2004). Our knowledge on the details of cortical neuronal wiring is rapidly accumulating (Gupta et al. 2000; Holmgren et al. 2003; Sporns and Zwi 2004; Stepanyants et al. 2004; Foldy et al. 2005; Kalisman et al. 2005; Song et al. 2005; Yoshimura and Callaway 2005; Yoshimura et al. 2005). However, such knowledge is limited on the synaptic contacts among a small number of neurons, and the topological pattern in which thousands or tens of thousands of neurons are wired together remains unknown. Different wiring topologies give rise to different degrees of clustering among neurons (how densely a population of neurons is mutually connected) and different mean path lengths (on average, how many synapses are present along the shortest path connecting a neuron pair), both of which can influence the temporal structure of synaptic inputs to each neuron in a population

Action Editor: Xiao-Jing Wang

K. Kitano (✉)
Department of Human and Computer Intelligence,
Ritsumeikan University, 1-1-1 Nojihigashi, Kusatsu,
Shiga 525-8577, Japan
e-mail: kitano@ci.ritsumei.ac.jp

T. Fukai
Laboratory for Neural Circuit Theory,
RIKEN Brain Science Institute, 2-1 Hirosawa, Wako,
Saitama 351-0198, Japan

and hence that of the output spike sequences. The connection probability between a pair of pyramidal neurons, for example, drops below 50% of the maximum possible value, typically when the distance between the pair becomes greater than 200–300 μm. The volume of such a small local region contains 10,000–100,000 neurons, a sufficient number of neurons for making different network topologies meaningful.

In the present study, we investigated how different kinds of network topologies influence spike statistics of individual neurons and spike coherence between neuron pairs in the model cortical network. In vivo, spontaneously firing cortical neurons are considered to be in a high conductance state, a condition generated by continuous bombardment of background synaptic inputs (Destexhe et al. 2001). This state typically exhibits high coefficient of variation (Cv) values that are close to, or even greater than, unity (Shadlen and Newsome 1998; Softky and Koch 1993). Attempts have been made to clarify the source of such variability, since it occurs ubiquitously in various regions of the cerebral cortex (Shinomoto et al. 2005) and may play an active role in cortical computations (Destexhe and Paré 1999; Fukai 2000; Maass et al. 2002; Wolfart et al. 2005). Stochasticity in spike generation (Chow and White 1996) is an unlikely source, since the neuronal spike generator faithfully converts input current to output spike trains (Mainen and Sejnowski 1995). Irregular output spikes of cortical neurons, therefore, reflect a certain stochastic nature of noisy synaptic inputs, such as independent noisy excitatory and inhibitory synaptic inputs (Destexhe et al. 2001) or transiently synchronous synaptic inputs superposed on noisy background inputs (Stevens and Zador 1998). However, the influences of neuronal wiring structure on the temporal structure of synaptic inputs have not been extensively studied.

Synchronization of output spikes is another important measure that characterizes the dynamical states of a neuronal network. For instance, in a randomly connected network of integrate-and-fire neurons and delta-function synaptic transmissions, the stable network state exhibits asynchronous spike firing in a regime of weak synapses, whereas it displays synchronous spike firing in a regime of strong synapses (Brunel 2000). The transitions occur sharply between the two types of the stable states (we note that the network also has other types of the stable state), when the synaptic strength crosses a certain critical value. It is intriguing to study whether and/or how such a state change may occur with other types of neuronal wiring, using realistic models of neurons and synapses.

To investigate how sensitive the variability or the synchronicity of neuronal activity is to local network structure, we systematically changed the topology of neuronal wiring in a two-dimensional model neuronal network. By rewiring synaptic connections, we varied the network topology from a locally clustered, regular network pattern to a randomly connected pattern. In an intermediate kind of topology, the network remains in a high-clustering arrangement, with a small fraction of long-range connections. These connections make the average path length between arbitrary neuron pairs sufficiently short. Such a network topology is called a "small-world" organization and appears in many biological and real-world networks (Watts and Strogatz 1998) including the functional network between various cortical regions (Achard et al. 2006).

2 Materials and methods

2.1 Neurons

Our model of cortical networks consisted of two types of neurons—excitatory and inhibitory. Both types of neurons had single compartments that were modeled by conductance-based membrane dynamics. Each excitatory neuron had a leak current (I_L), spike-generating sodium and potassium currents (I_{Na} and I_K), and a non-inactivating potassium current (I_M), all of which followed the channel kinetics formulated by Destexhe and Paré (1999). The dynamics of the membrane potential obeyed the following equation:

$$C_m dV/dt = -I_L - I_{Na} - I_K - I_M - I_{syn} - I_{bg},$$

where I_{syn} and I_{bg} represent synaptic input from other neurons and background synaptic input, respectively. These currents are defined below. The conductance densities of these currents were set to g_L=0.045 mS/cm^2, g_{Na}=50.0 mS/cm^2, g_K=5.0 mS/cm^2, and g_M=0.07 mS/cm^2. The reversal potentials were set to E_L=−80 mV, E_{Na}=50 mV, and E_K=−90 mV. Fast-spiking interneurons (FS neurons) were modeled as having Kv3.1–Kv3.2 potassium channels (Erisir et al. 1999),

$$C_m dV/dt = -I_L - I_{Na} - I_K - I_{syn} - I_{bg},$$

where I_{syn} and I_{bg} were similar to those in the excitatory neuron model. These neurons could fire at high frequencies, even frequencies greater than 200 Hz. The activation and inactivation functions for the gating variables were shifted by −1 mV in both the sodium and potassium channel model components, as given in Erisir et al. (1999).

2.2 Synapses

The excitatory synaptic currents were mediated by components modeled after characteristics of AMPA (I_{AMPA}) and NMDA (I_{NMDA}) receptors, and the inhibitory currents were mediated by components modeled after characteristics of GABA-A receptors (I_{GABA}). The AMPA synaptic current

exhibited short-term depression of transmitter release in the condition of repetitive activation of the synapses (Tsodyks and Markram 1997). Depressing synapses were modeled as

$$I_{AMPA} = g_{AMPA} w (V - E_{AMPA}),$$

$$\tau_{inact} dw/dt = -w + U \, r \, \delta(t - t_{pre}),$$

$$\tau_{rec} dr/dt = (1 - r - w),$$

where w represents the fraction of the "effective" state, r the fraction of the vesicles available at presynaptic terminals, U the probability of transmitter release, and t_{pre} the times of presynaptic spikes. The time constant of inactivation was set to τ_{inact}=2.7 ms. At cortical AMPA synapses, recovery from short-term depression shows a range of time constants (Petersen 2002). Therefore, the values of τ_{rec} were determined according to a Gaussian distribution of 500± 150 ms (mean±SD). The maximum conductance was set to g_{AMPA}/g_L=0.504, which corresponds to an EPSP of 0.8 mV at a resting potential of about −80 mV. In some simulations, we multiplied the value of g_{AMPA} by a scaling factor. Typically, we took 1.125×g_{AMPA} and 1.25×g_{AMPA}, which yielded EPSPs of 0.9 and 1.0 mV at the resting potential, respectively.

The NMDA synaptic current was modeled by first-order kinetics as,

$$I_{NMDA} = g_{NMDA} r f(V) (V - E_{NMDA}),$$

$$dr/dt = \alpha T (1 - r) - \beta r,$$

$$f(V) = \left(1.0 + 0.28 \left[Mg^{2+}\right] e^{-0.062V}\right)^{-1},$$

where $[Mg^{2+}]$=1.0 mM and E_{NMDA}=0 mV (Jahr and Stevens 1990). T is a binary variable, which takes a value of 1 for 1 msec after an occurrence of a presynaptic spike, otherwise it takes a value of 0 (Destexhe et al. 1998). We set α and β equal to 0.5 and 0.007, respectively, which gave rise to decay time constants of 1.97 and 143 ms, respectively (Destexhe et al. 1998). The maximum conductance g_{NMDA} has been reported to range from 0.2 to 0.4 nS (Koch 1999), or from 0.0126 to 0.0252 in the unit of g_L, if the total area of a cell is estimated to be about 3.5×10^{-4} cm^2 (Destexhe et al. 2001). Therefore, we randomly drew a value for g_{NMDA} for each synapse from a Gaussian distribution having a mean of 0.0189 (0.3 nS) and a standard deviation of 0.0063 (0.1 nS). The GABAergic synapses were represented by first-order kinetics as,

$$I_{GABA} = g_{GABA} r (V - E_{GABA}),$$

$$dr/dt = \alpha T (1 - r) - \beta r,$$

where α=5.0, β=0.1, E_{GABA}=−75 mV, and g_{GABA}/g_L= 0.094. As is the case with the AMPA synapses, we multiplied the value of g_{GABA} by a scaling factor in some simulations.

2.3 Background synaptic input

Both excitatory and inhibitory neurons received background synaptic inputs in our model. To study spike sequence statistics, we employed a point-conductance model that mimics highly variable spike discharges of in vivo cortical neurons (Destexhe et al. 2001). The background synaptic current I_{bg} consisted of excitatory and inhibitory components:

$$I_{bg} = g_e(t)(V - E_{AMPA}) + g_i(t)(V - E_{GABA}).$$

Fluctuations in $g_e(t)$ and $g_i(t)$ were modeled as,

$$dg_e(t)/dt = -(g_e(t) - g_{e0})/\tau_e + \eta_e(t),$$

$$dg_i(t)/dt = -(g_i(t) - g_{i0})/\tau_i + \eta_i(t),$$

where g_{x0} and τ_x (x=e or i) represent the average conductance and the time constant of synaptic integration, respectively, and $\eta_x(t)$ introduces Gaussian white noise. The noise satisfies $<\eta_x(t)>=0$ and $<\eta_x(t)\eta_x(t')>=D_x\delta(t-t')$, where D_x is the diffusion coefficient and $<>$ denote temporal averaging.

Stochastic processes of $g_x(t)$ are known to give a Gaussian distribution with mean g_{x0} and variance $\sigma_x^2 = D_x\tau_x/2$. The values of parameters were set as g_{e0}=12Q nS, σ_e=3$Q^{1/2}$ nS, τ_e=2.7 ms, g_{i0}=57Q nS, σ_i=6.6$Q^{1/2}$ nS, and τ_i=10.5 ms to reproduce membrane fluctuations in layer IV pyramidal neurons (Destexhe et al. 2001). Note that Q rescales the intensity of background synaptic input to adjust the net amount of membrane fluctuations in an appropriate range in the presence of recurrent synaptic input; typically, Q=0.8.

2.4 Network structure

Our cortical network consisted of 4,096 excitatory and 1,024 inhibitory neurons. The excitatory and inhibitory neurons were arranged in a two-dimensional space on grids of 64×64 and 32×32 arrays, respectively. Thus, the density of excitatory neurons was four times larger than that of inhibitory neurons. In the regular network topology, each excitatory or inhibitory neuron made synaptic contacts with all neurons within a distance of four lattice-lengths, which implies that the excitatory and the inhibitory neuron projected to 48 excitatory and 12 inhibitory neurons, respectively. Thus, the connection probability between modeled pyramidal neurons was about 1.2%, which is within the reported range of experimental observations for local cortical circuits (Holmgren et al. 2003). In an analysis,

Fig. 1 Network connectivity in a two-dimensional small-world ▶
network paradigm. (a) For different values of a rewiring probability
p, typical connectivity of sampled neurons is illustrated. *Lines*
represent in-coming "fibers" to neurons located on a two-dimensional
grid. As p increases, a given neuron receives more afferents from
distant neurons. (b) Indicated are the average shortest path length and
clustering coefficient, each of which is normalized by a value when
p=0. The average shortest path length decreased at very small p
values, whereas the clustering coefficient remained large for a
comparably large p. Connectivity patterns having short path lengths
and a large clustering coefficient are referred to as small-world
networks

the conduction delay in synaptic transmissions was
increased in proportion to the distance between presynaptic
and postsynaptic neurons. We set the delay equal to 1 ms
between a neuron pair separated by a distance of 64 units.

We randomly rewired the synaptic connections of the
regular neuronal network according to the following rule. Let
p be the probability of rewiring. We selected the synapses of
axons sent by each neuron with a probability of p, and
rewired the selected synapses to randomly chosen neurons
irrespective of the distance between the neuron pairs. The
probability p defined the topology of neuronal wiring in the
network. At p=0, the network remained a regular neuronal
network (Fig. 1(a), top). At p=1, all synapses were
randomly rewired, hence we obtained a random network
(Fig. 1(a), middle). If p took on an intermediate but
relatively small value, a small fraction of the synaptic
connections were long-range connections, while most of
them were short-range local connections (Fig. 1(a), bottom).
This kind of network topology is called a "small-world"
network (Watts and Strogatz 1998). In most of the present
simulations, we only rewired excitatory synaptic connec-
tions. However, we also rewired inhibitory synapses in some
simulations to explore how the topology changes in both
synapse types may influence activity of the network.

Network topology can be characterized by two statistical
measures for connectivity: one is the average, shortest path
length (steps) between neuron pairs, $L(p)$; and the other is
the clustering coefficient, $C(p)$. In calculating $L(p)$, we
counted the number of steps from one neuron to another
along the shortest synaptic pathway and averaged these
numbers over all neuron pairs. The clustering coefficient
$C(p)$ represents the probability that two neurons connected
to another neuron are again connected. A regular network is
characterized by a large $L(p)$ and a large $C(p)$, whereas both
quantities are small in a random network. By contrast, a
small-world network has a small $L(p)$ and a large $C(p)$
(Fig. 1(b)). As Fig. 1(b) shows, the normalized $L(p)$ is
rapidly reduced by the increase in p, whereas the
normalized $C(p)$ remains relatively large in comparison
with $L(p)$. In the present study, we set p=0 (regular), 0.05
(small-world), and 1.0 (random) as typical examples.
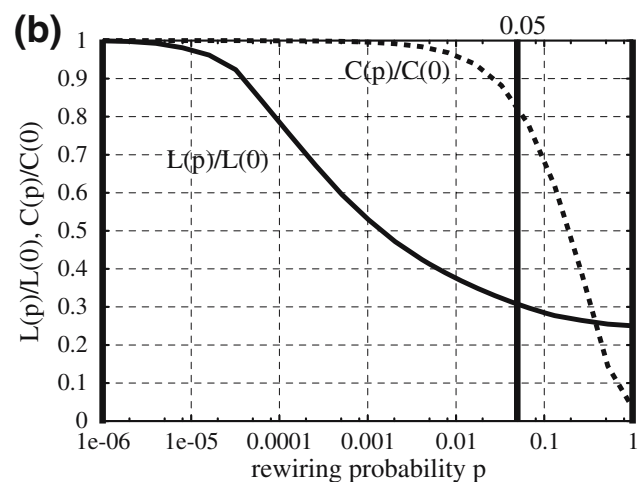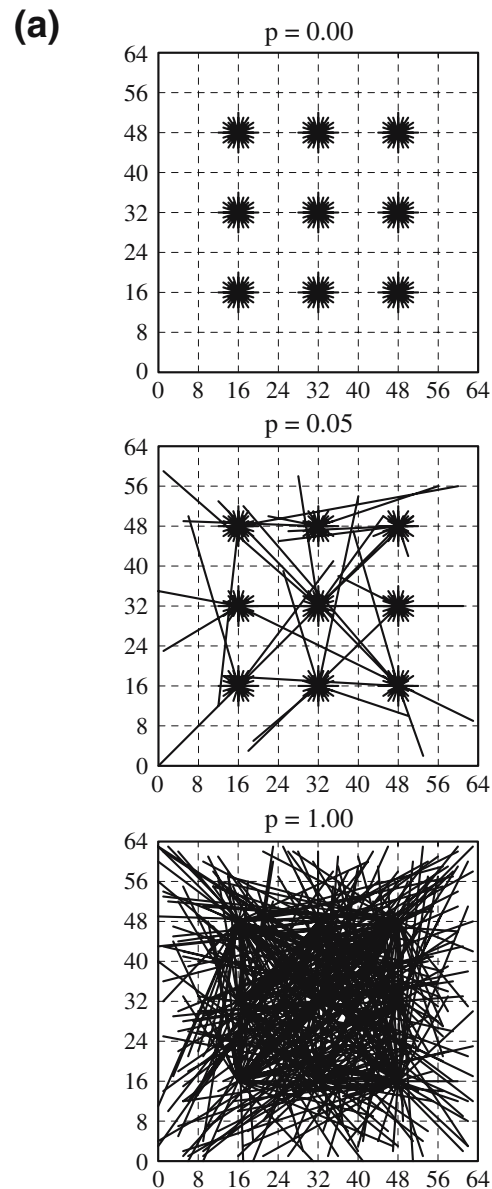
2.5 Spike data analyses

We analyzed the statistical properties of neuronal activity obtained in the numerical simulations using several statistical measures often used in neurophysiological experiments. First, we calculated the ISIs of spike sequences emitted of individual neuron firing. Then, we analyzed the Cv, which is defined as the ratio of the standard deviation of the ISI distribution, σ_T, to the average, $<T>$, namely,

$$Cv = \sigma_T / \langle T \rangle.$$

This quantity is widely used for characterizing the variability of neuronal activity. If a spike sequence obeys a Poisson process, the Cv takes on a value of 1. By contrast, if spikes occur periodically, both measures become 0.

2.6 Analysis of spike synchrony

To analyze the relationship between the circuit structure and the global network activity, we examined a degree of spike synchronization in the model network. As a measure of spike synchronization, we applied the coherence measure proposed by Wang and Buzsáki (1996). Firstly, we binned spike sequences such that each bin contained at most one spike to obtained 01-sequences for the pair of neurons, $\{X_i\}$ and $\{Y_i\}$ ($i=1, 2, \ldots, N_b$). N_b is the number of bins in a 01-sequences. Then, we calculated the coherence measure for the pair,

$$\kappa_{XY} = \frac{\sum_{i}^{N_b} X_i Y_i}{\sqrt{\sum_{i}^{N_b} X_i \sum_{i}^{N_b} Y_i}}.$$

We obtained values of the measure for all possible pairs and regarded an average value as a measure of global spike synchronization. The bin size used for the analysis was set as 4 ms.

2.7 Numerical simulations

Simulation program was written in C and parallelized with MPI programming. Simulations were conducted on a PC cluster that consisted of eight or 16 Pentium4 CPUs.

3 Results

We conducted numerical simulations of spontaneous activity in a recurrent network of modeled excitatory and inhibitory neurons and accumulated 50 sec of spike data. We adopted the excitatory neuron that was modeled by Destexhe and Paré (1999) to account for the spike variability in in vivo cortical neurons. In our regular network, the excitatory and inhibitory neurons distributed in a two-dimensional space were arranged on individual grids having either a 64×64 or a 32×32 lattice, respectively. Thus, the neuronal spatial density was four times larger in the excitatory neuron population than in the inhibitory neuron population. We introduced excitatory-to-excitatory, excitatory-to-inhibitory, inhibitory-to-excitatory, and inhibitory-to-inhibitory synaptic connections to all neurons located in the local neighborhood of each excitatory or inhibitory neuron. This arrangement resulted in a locally connected regular network. Then, we identified each excitatory-to-excitatory synapse with probability p, and rewired it to a randomly chosen excitatory neuron regardless of the distance to that neuron (Fig. 1(a)). Through this rewiring procedure, the topology of neuronal wiring could gradually be changed from a topology characterizing a regular ($p=0$) network to one characterizing a random ($p=1$) network. Between the two extremes, the excitatory-neuron network displayed the small-world property, which is characterized by a large cluster coefficient and a small average path length (Fig. 1(b)). Next, we tested how the statistical properties of spike outputs generated by excitatory and inhibitory neurons might change with changes in the wiring pattern. Unless otherwise stated, the only difference between our different network models was the neuronal wiring defined by p. Other parameters in the model remained unchanged.

3.1 Time courses of neural activity

Figure 2 shows activity snap shots of excitatory neurons in two-dimensional networks with different network topologies (64×64 neurons). The maximum conductance of excitatory synapses was $1.125 \times g_{AMPA}$. The gray-scale plot in a given snap shot represents the number of spikes elicited from four neighboring neurons located at each spatial position within the corresponding interval of 20 ms. In the regular network ($p=0$), neuronal activity induced spontaneously in a local area slowly propagated to neighboring neurons through the localized patterns of excitatory synaptic connections between neighbors. The propagating activity initially grew, but it finally disappeared 200–300 ms after its initiation due to the depressing property of AMPA synapses. Such temporally localized activities appeared intermittently in the regular network. Similar spontaneous neuronal activities were also observed in a small-world network obtained at $p=0.05$. Neuronal activations at a local site spread over a broader region in this

Fig. 2 Spiking activities in neuronal networks having different wiring topologies. The AMPA synaptic conductance was set to $1.125 \times g_{AMPA}(=0.567)$. "Snap shots" of the activity of 64×64 pyramidal cell arrays over time are shown in each 20 ms time window. The rewiring parameter was set at (**a**) $p=0$ (regular network), (**b**) 0.05 (small-world network) and (**c**) 1.0 (random network). The same set of random spike trains was used for noisy background synaptic inputs in all three neuronal networks
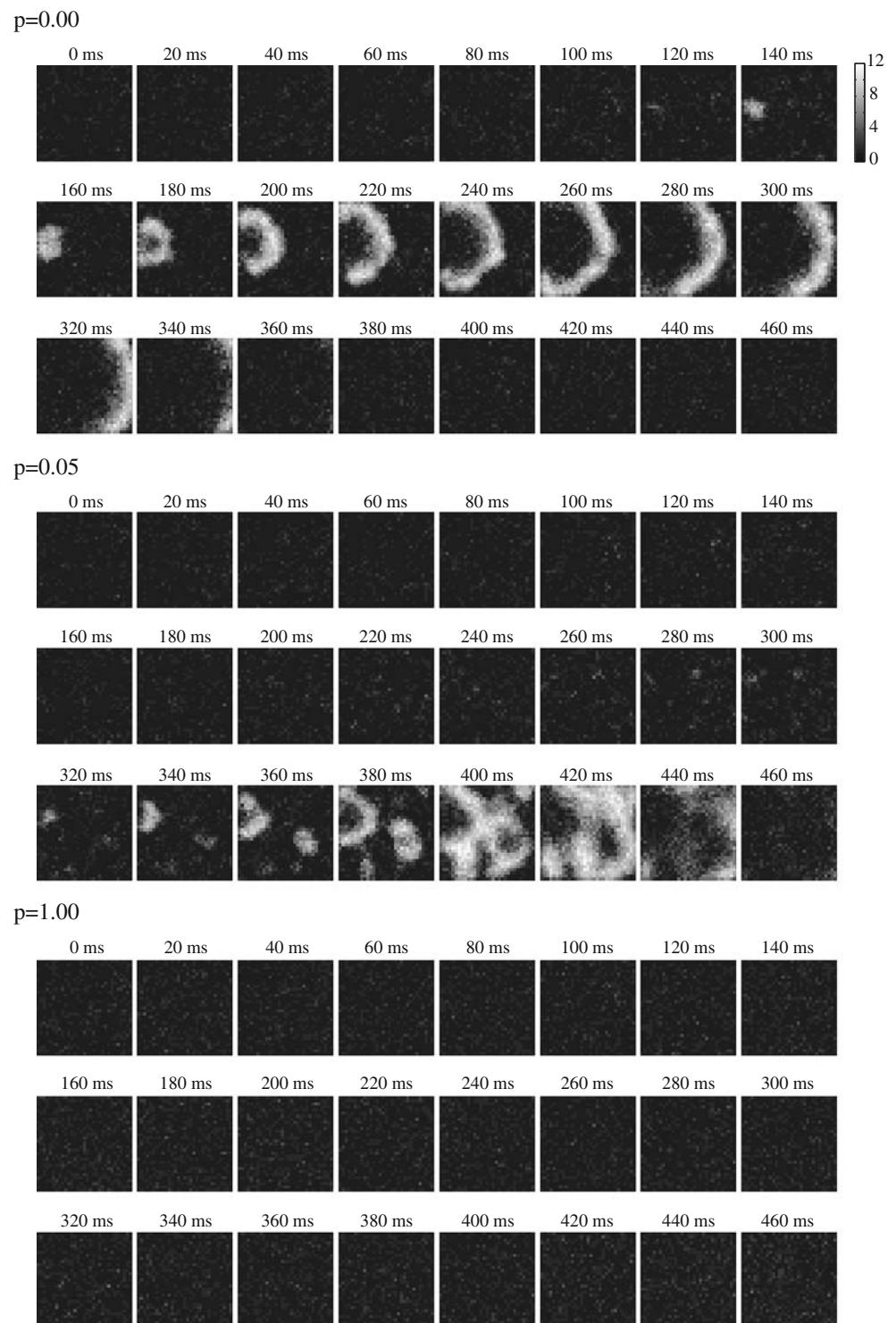
network than in the regular network. It is, however, noted that the spatiotemporal activity pattern depended significantly on the maximum conductance of excitatory synapses in the small-world network topology. For instance, neuronal activities were spatially and temporally much more localized at smaller values of the conductance (data not shown).

We will study later how neuronal activity depends on the strength of recurrent excitation in detail. In the random network ($p=1$), individual neurons fired irregularly without creating temporal clusters of spikes.

Figure 3(a) shows the time course of the membrane potential of a modeled excitatory neuron and the sum of all
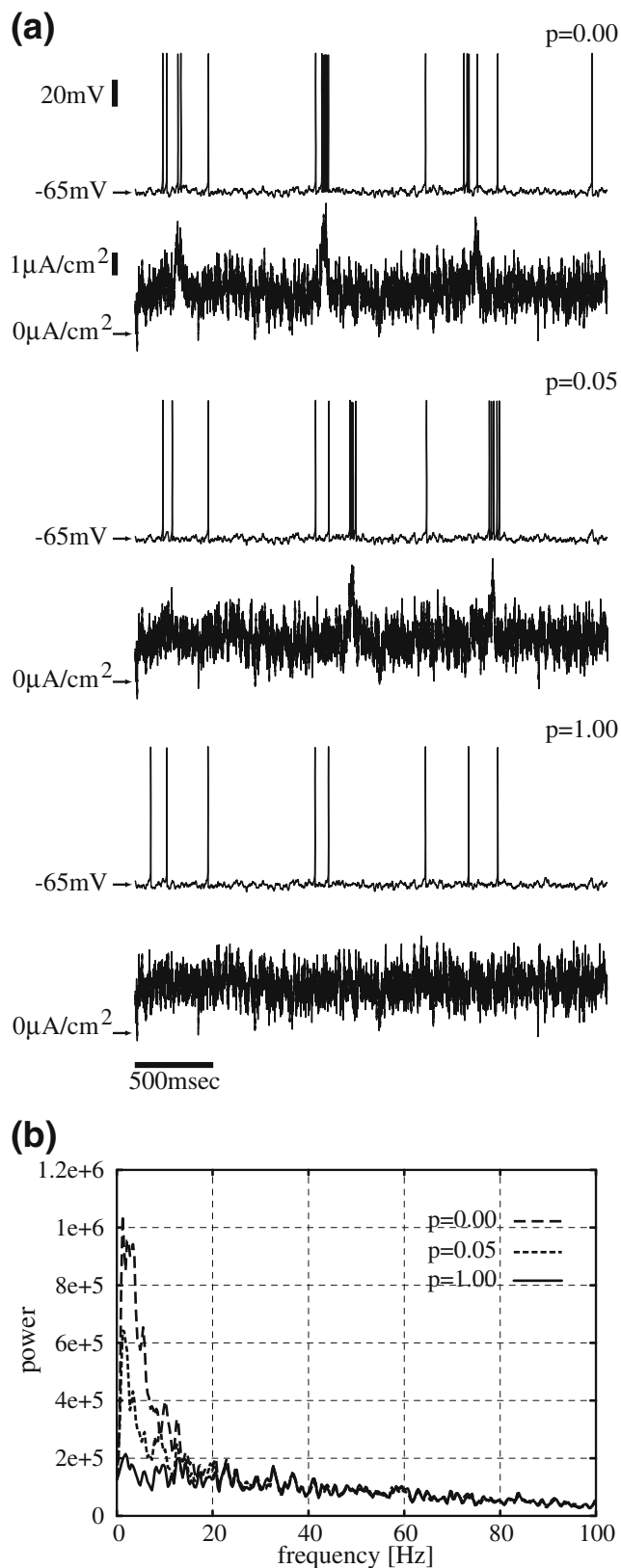
(a)

(b)

in the simulations. Therefore, fluctuations in the total current essentially represented those in EPSCs. In the highly clustered networks ($p=0$, $p=0.05$), bursts of action potentials were elicited intermittently by coincident arrivals of presynaptic spikes, as indicated by the large fluctuations in the total current. By contrast in the random neuron network, large fluctuations and spike bursts were rare. To characterize the frequency of large current fluctuations, we calculated power spectra of the total ionic current (Fig. 3(b)). While all three neuronal networks exhibited frequency components higher than 10–20 Hz with almost identical power, the lower frequency components displayed stronger power when $p=0$ and $p=0.05$ than when $p=1$. Since the peaks of the low-frequency components were located at about 1.2 Hz in the highly clustered networks ($p=0$, $p=0.05$), the intervals between the successive arrivals of coincident presynaptic spikes were typically 800–1,000 ms.

3.2 Network topology and spike variability

To further characterize the different network activities represented by bursts of output spikes, we calculated the distributions of ISIs from the spike trains of the individual neurons. Figure 4(a) represents the ISI histograms summed over all excitatory neurons. As evident from the figure, ISIs longer than ~100 ms occurred at almost equal frequencies in all types of neural networks. However, the counts of shorter ISIs grew rapidly as p decreased.

The irregular firing of in vivo cortical neurons is often characterized by the Cv. Therefore these statistical quantities are of particular interest to experimental neuroscientists. As shown below, the Cv values of excitatory neurons ranged from a low of ~0.7 to a high of ~1.5 in our numerical studies. The ISI histogram of high-Cv neurons displayed a remarkable peak at short ISIs (<~50 ms) along with a long tail extending out to more than 1 s (inset of Fig. 4(a), upper panel). By contrast, the ISI histogram of low-Cv neurons did not display this peak at short ISIs, indicating that these neurons generated bursts of spikes less frequently (inset of Fig. 4(a), bottom panel).

A specific network topology significantly enhanced the variability of neuronal activity in our recurrent network models. In Fig. 4(b), we display the Cv values of ISIs for all excitatory and inhibitory neurons. The top and bottom
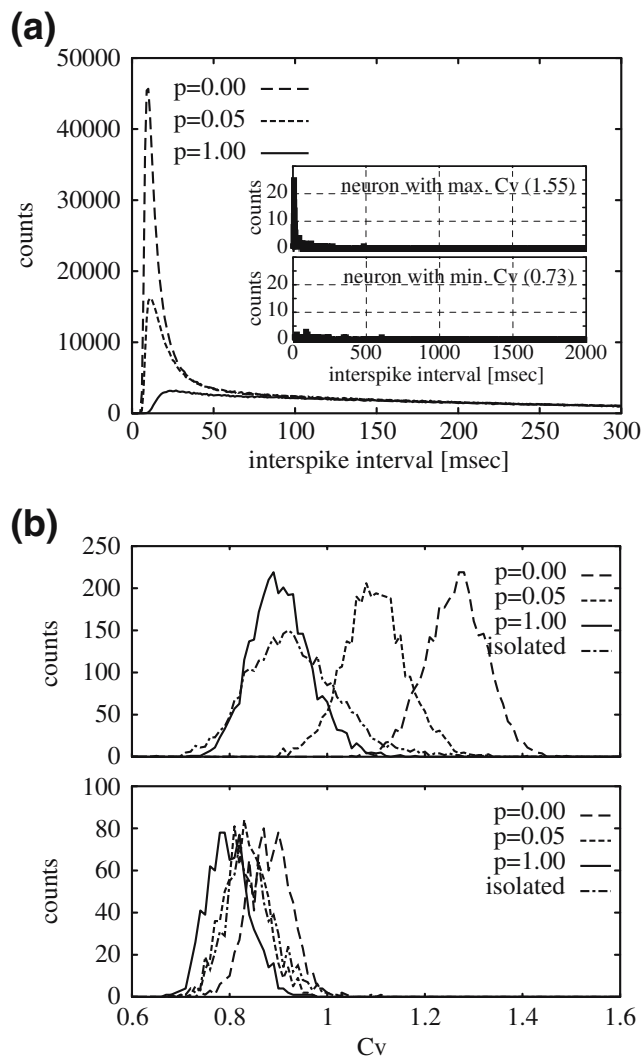
intrinsic and synaptic currents. The total ionic current was obtained by clamping the membrane potential at −75 mV (i.e., reversal potential of the GABAergic synaptic current)

(a)

(b)

Fig. 4 Inter-spike interval histograms of modeled neurons in the three networks. (**a**) The ISI histograms summed over all excitatory neurons show distinct profiles for the different network topologies. In networks with small p values, the frequency of short ISIs (<30 ms) is considerably greater than that in networks with progressively larger p values. (The average ISI was 150 ms for $p=0$ and 168 ms for $p=$ 0.05.) *Inset* shows ISI histograms for pyramidal neurons with a large or a small Cv value. The upper histogram was obtained from the neuron that exhibited the maximum value of Cv (1.55) in the regular network ($p=0$), whereas the lower one was from the neuron with the minimum Cv (0.73) in the random network ($p=1$). (**b**) Dependence of Cv distributions on network connectivity. The *top and the bottom panels* show the distribution over all excitatory or inhibitory neurons, respectively. The "isolated" distribution in each panel is obtained when the corresponding neurons only receive background synaptic inputs without recurrent synaptic inputs

panels display the excitatory and inhibitory neurons in the different network types, respectively. In both panels of the figure, the curves of "isolated" show the Cv distributions of excitatory and inhibitory neurons in the network where all synaptic connections were decoupled, namely, all the neurons in the network were driven only by background

synaptic inputs. The Cv distribution in the random network was almost unchanged from that of the decoupled neurons, indicating that this network topology did not create an extra amount of variability. By contrast, the Cv values shifted to significantly larger values in the small-world network. These values distributed within the largest value range of the regular network. The regular and small-world networks, in particular, exhibited average Cv values that were greater than unity. The Cv values of these networks were large, because their output spike trains consisted of a mixture of short and long ISIs (Fig. 4(a)). The Cv distributions of inhibitory neurons were not modulated much by the network structure in comparison with excitatory neurons.

3.3 Distributed spike synchronization in different network topologies

In addition to spike variability, the degree of spike synchronization is a frequently studied characteristic of neural activity. To analyze how network topology affects a spatial distribution of spike synchronization, the degree of spike synchronization for a pair of neurons can be measured by a coherence index (Wang and Buzsáki 1996). Figure 5(a–c) displays the coherent indices averaged over all the excitatory neuron pairs separated by a given spatial distance. Each figure shows the indices obtained in the three different networks with a magnitude of the AMPA synapses. Each symbol or error bar represents the average and standard deviation, respectively. Figure 5(a) indicates the coherence indices as functions of distances between neuron pairs in the networks with a reference synaptic strength g_{AMPA}. In this case, the regular network exhibited the strongest synchrony among the three networks although the synchrony was observed only at adjacent pairs. Figure 5(b) and (c) show the indices for the networks with increased synaptic strengths of $1.125 \times g_{AMPA}$ and $1.25 \times g_{AMPA}$, respectively. In the regular network, the coherence index took a maximum value between nearby cells and rapidly dropped off as the spatial separation was increased. The coherence index of the small-world network deteriorated moderately compared with that of the regular network, and remained to be relatively large even between distant pairs. The degree of spike synchronization was, as expected, independent of the spatial separation between a neuron pair in the randomly-connected network. Thus, the profile of the index for each the network was preserved even though the synaptic strengths were increased. The small-world network, however, showed the largest value of the index in Fig. 5(b) whereas the degree of synchrony for the random network became the largest in Fig. 5(c). The pairwise synchrony was enhanced in different manners, depending on the network topology.
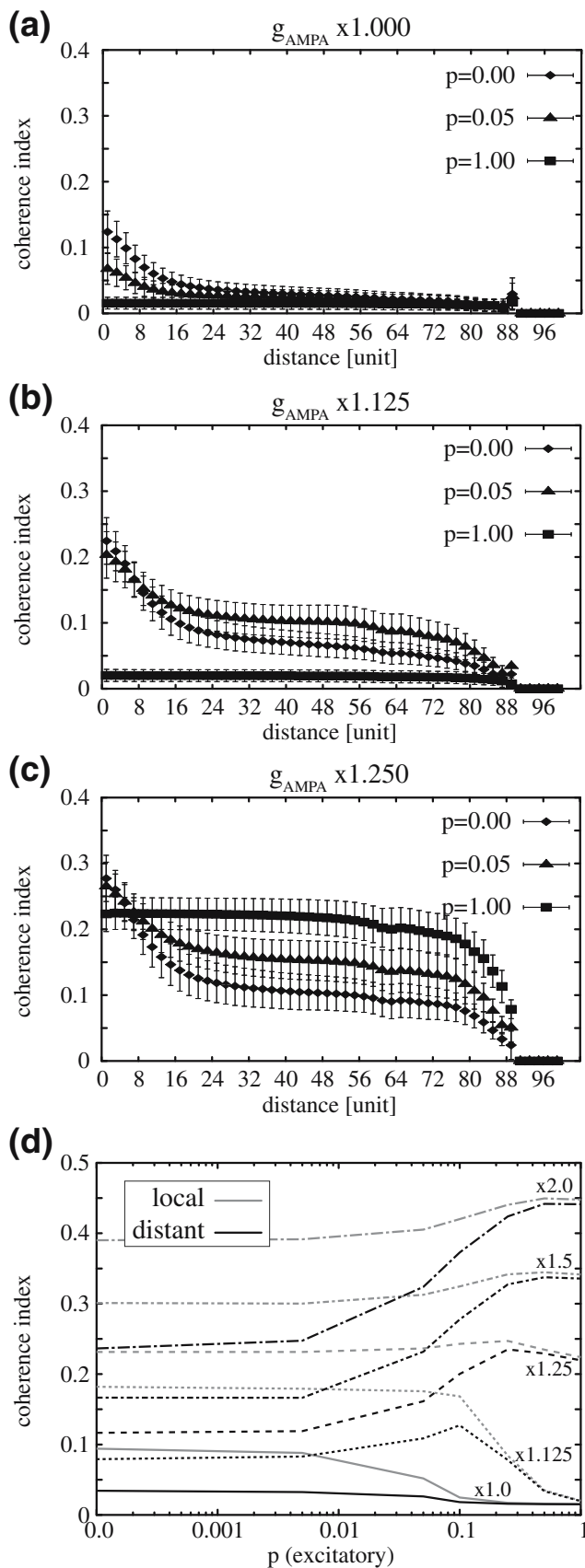
(a)

(b)

(c)

(d)

Fig. 5 Dependence of spike synchronization on network connectivity and synaptic strengths. (**a**) The degree of spike synchronization in networks with a strength of AMPA synapses, g_{AMPA}(=0.504), is expressed as a function of spatial distances between excitatory neuron pairs. A *symbol and an error bar* indicate an average and a standard deviation over neuron pairs with a specific distance, respectively. Three kinds of symbols correspond to results in the networks with different topologies. (**b**) A similar plot to (**a**) for $1.125 \times g_{AMPA}$(=0.567). (**c**) A similar plot to (**a**) for $1.25 \times g_{AMPA}$(=0.63). (**d**) Local and distant pairs exhibited different dependences on the network topology and synaptic strength. The *gray lines* indicate the coherence indices averaged over all neuron pairs located within eight unit lengths. The *black lines* are the average coherence over the remaining pairs. The *numbers* represent the factors multiplied by the synaptic strength

We further examined whether local and distant neuron pairs exhibit different dependences of synchrony on the network topology and synaptic strength (Fig. 5(d)). In the analysis, we defined a neuron pair as local or distant if the spatial separation between them was within or greater than eight unit lengths, respectively. In the figure, the curves labeled "local" or "distant" represent the coherence indices averaged over all local or distant pairs in the network, respectively. As the AMPA synapses were strengthened, the coherence indices were increased monotonically in both local and distant pairs. At a given strength of the AMPA synapses, the differences between the local and distant coherence indices were relatively large for small p. As p increased, however, the local and distant coherence converged since the physical distance is meaningless in the random network. In the local pairs the spike coherence was moderately changed with the changes in p. By contrast, the average coherence in the distant pairs was significantly changed with the changes in p, especially for strong AMPA synapses ($> \times 1.25$), presumably due to the existence of long-range connections.

3.4 Combined effects of excitatory-to-excitatory network topology and synaptic strength

The results shown in Fig. 5 demonstrated that the network activity depends highly on the combination of the network topology and the synaptic strength. Below, we analyze the dependency of Cv, the coherence index and firing rate on the network topology and the strength of AMPA and GABAergic synapses. Here, we examined the following three cases: (1) Only the strength of excitatory synapses are changed keeping that of inhibitory ones unchanged; (2) only the strength of inhibitory synapses are changed keeping that of excitatory ones unchanged; (3) the magnitudes of both types of synapses were changed keeping the ratio between the AMPA and GABAergic conductances unchanged. We scaled the relative conductance

Fig. 6 Spike variability and spike synchrony modulated by the network topology and synaptic strength. Here, p refers to the probability of rewiring excitatory synapses. (**a**) The average value of Cv was plotted against the rewiring probability at various magnitudes of AMPA and GABA synapses. *Magenta lines* represent the results obtained by changing only the strength of AMPA synapses, which was multiplied by a constant scaling factor chosen from (1.125, 1.25, 1.5, 2.0). *Cyan lines* represent the results when only the strength of GABAergic conductance was changed. *Green lines* indicate the result when both types of synapses were changed with the same constant multiplied. *Error bars* represent the standard deviations. (**b**) The average spike coherence was plotted in a similar manner. The coherence indices were averaged over all possible neuron pairs. (**c**) Similarly, we plotted the firing rate averaged over all excitatory neurons in each network topology

of the AMPA and GABAergic synapses with factors (1.125, 1.25, …, 2.0) in the case (1) and (1.125^{-1}, 1.25^{-1}, …, 2.0^{-1}) in the case (2). It was unchanged in the case (3). We rewired only excitatory synapses, but not inhibitory ones. We will later study the effect of simultaneously rewiring of both synapse types.

We fitted the Cv distributions by Gaussian distributions. Then, the means and standard deviations of these distributions were plotted against the rewiring probability for various magnitudes of AMPA and GABAergic recurrent synapses (Fig. 6(a)). In the case (1), for relatively weak AMPA synapses (×1.0 and ×1.125), the average Cv value was decreased as the network topology approaches a random one. With increased synaptic weights (×1.250 and ×1.5), ISI was highly variable and the Cv value was saturated at about 1.5. The ISI histograms resembled those presented in Fig. 4(a) (data not shown), and the increase in Cv values was due to the increase in bursts of spikes. In the case (2), increasing the maximum conductance of GABAergic synapses suppressed the variability of spike trains in the regular networks, but this suppression was generally not so significant. The results in the case (3) differed little from those in the case (1).

We analyzed the spike synchrony in a similar manner (Fig. 6(b)). In general, synchronization was greatly enhanced as we strengthened the AMPA synapses. However, the way the spike coherences depend on the synaptic strength differed qualitatively in different wiring topologies. When $p > 0.1$, the coherence index displayed a large change at a value between $1.125 \times g_{AMPA}$ and $1.25 \times g_{AMPA}$ as we increased the synaptic strength. This change may represent a phase transition between synchronous and asynchronous firing states in random networks (Brunel 2000). However, confirming whether this is really the case requires analytic studies of the network dynamics, which are beyond the scope of this paper. When $p < 0.1$, changing the synaptic strength varied the degree of synchrony in a graded manner. Thus, the spike coherence depends on the strength of recurrent connections only moderately in the regular or the small-world network topology.
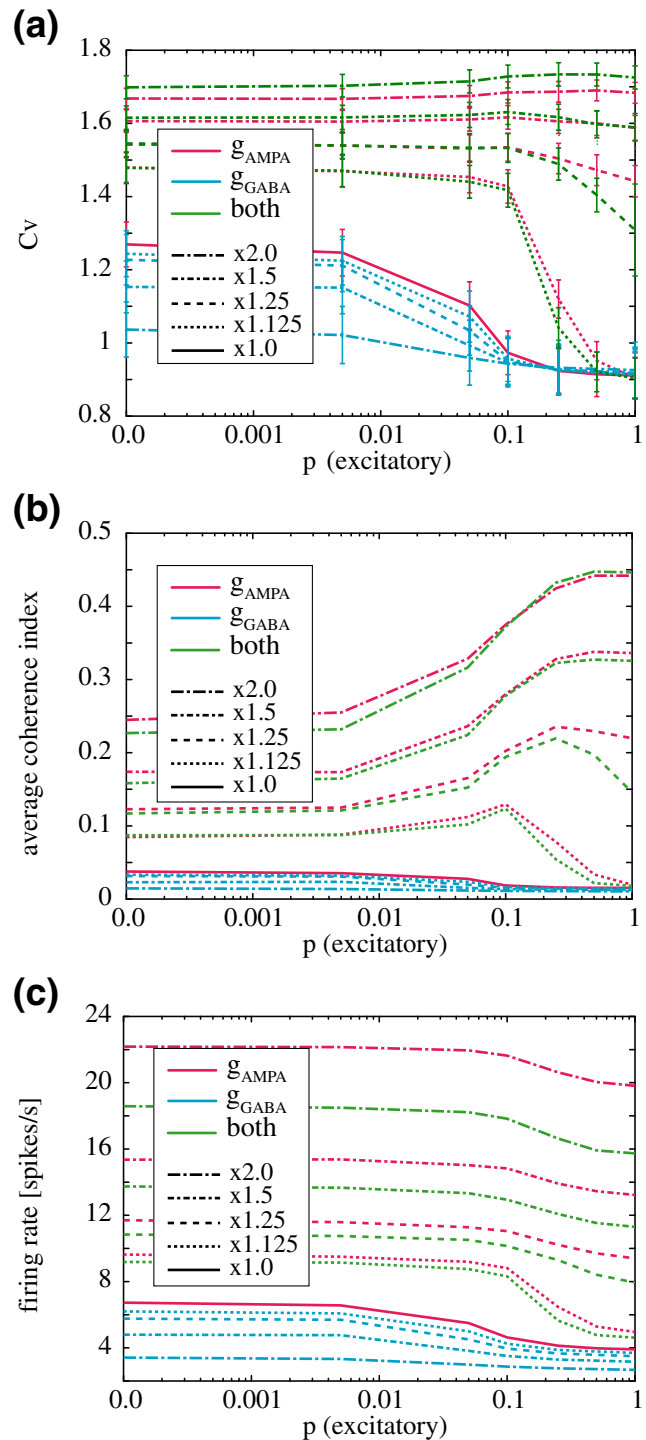
At a given excitatory synaptic strength, there exists a unique topological pattern that maximizes the coherence measure. For example, with the maximum conductance of $1.125 \times g_{AMPA}$, the spike coherence was maximized at $p = 0.1$. With a stronger maximum conductance, the spike coherence was maximized in a network topology closer to the random one. Increasing the GABA conductance slightly

suppressed the average spike coherence. When we strengthened both types of synapses, the coherence indices showed a network topology-dependence similar to that exhibited when we only strengthened the AMPA synapses.

The average firing rate also depended on the network topology, but this dependency was relatively weak at all values of the synaptic strength (Fig. 6(c)). As shown above, increasing the GABAergic conductance concurrently with the AMPA conductance had little effect on Cv and the spike coherence. However, such a change significantly decreased the average firing rate of excitatory neurons, especially in the network consisting of strong synaptic connections.

3.5 Effects of rewiring other types of excitatory and inhibitory synapses

So far, we have analyzed the activity patterns induced by rewiring only excitatory-to-excitatory (e–e) synapses. However, the present network also contains excitatory-to-inhibitory (e–i), inhibitory-to-inhibitory (i–i), and inhibitory-to-excitatory (i–e) synapses. We investigated the effects of rewiring these types of synaptic connections on neuronal firing patterns. We rewired those synapses by the same rewiring procedure as previous. Increasing the strength of AMPA synapses enhanced the average Cv value (Fig. 7(a)) and the average coherence index (Fig. 7(b)) in all types of neuronal rewiring. Rewiring all types of synapses simultaneously reduced both spike variability and spike synchrony to some degree at relatively large values of p. However, these manipulations kept the essential behavior of networks unchanged. Rewiring only AMPA synapses on excitatory and inhibitory neurons also reduced the variability and synchrony at a smaller degree. Rewiring only GABAergic synapses had little influence on neuronal firing patterns, and the network behavior was essentially governed by regularly-wired excitatory synaptic connections.

3.6 Effect of conduction delays in synaptic transmission

We investigated how the conduction delay in synaptic transmissions alters the statistical properties of network activity. For this purpose, we introduced distance-dependent conduction delays such that the delay was 1 ms in a neuron pair separated by 64 unit lengths. Figure 8 displays Cv and the average spike coherence obtained by varying the rewiring probability and AMPA synapse strength. For relatively weak AMPA synapses, the presence of conduction delays did not qualitatively change the dependence of Cv on the network topology (compare Fig. 8(a) with Fig. 6(a)). However, unlike in the previous simulations without conduction delays, Cv was increased monotonically as $p \rightarrow 1$ if the synapses were strong enough. By contrast, the conduction delays hardly changed how the spike
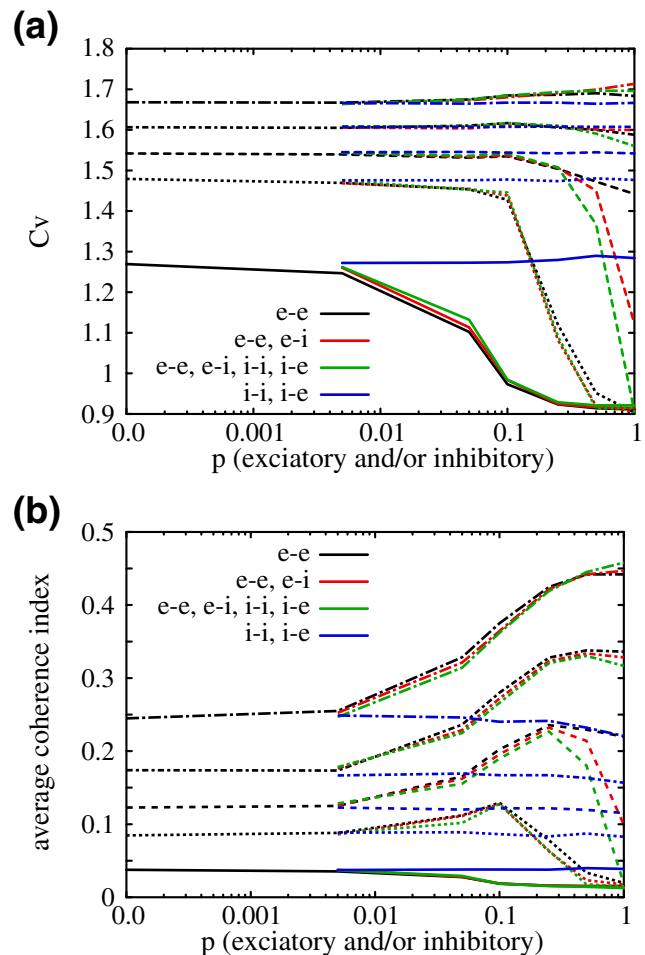

Fig. 7 The effects of rewiring all types of synapses. (**a**) The average values of Cv and (**b**) those of spike coherence. In both panels, the *insets*, "e–e", "e–i", "i–e" and "i–i", refer to random rewiring of excitatory-to-excitatory, excitatory-to-inhibitory, inhibitory-to-excitatory, and inhibitory-to-inhibitory synapses, respectively. Here, we rewired all synapse types designated in the inset simultaneously according to the same rule as applied to excitatory synapses in Fig. 6. In addition, the strength of AMPA synapses was multiplied by the same set of scaling factors as used in Fig. 6

coherence depends on the network topology and synaptic conductance (compare Fig. 8(b) with Fig. 6(b)).

4 Discussion

The statistical properties of neuronal activity may provide a clue for understanding the dynamics of neuronal responses and the nature of input they receive in the brain. Several experimental studies have reported highly variable cortical neuron activity (Shadlen and Newsome 1998; Softky and Koch 1993). We have investigated to what extent the spatiotemporal patterns and the statistical nature of spiking activity might depend on the topology of neuronal wiring in two-dimensional neuronal network models. The neuronal
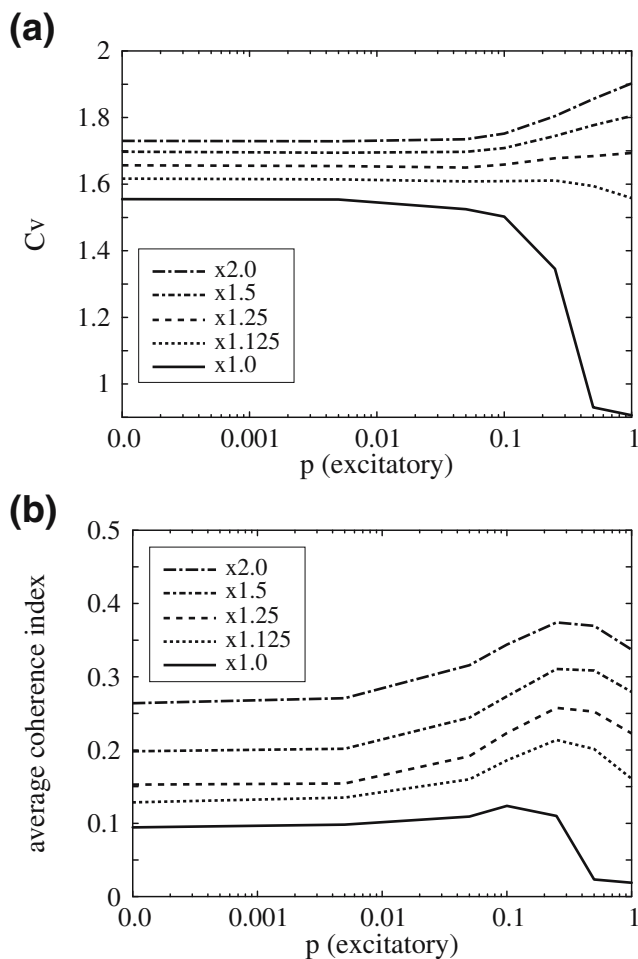
(a)

(b)

Fig. 8 The effect of delays in the synaptic transmission. The average values of Cv (**a**) and spike coherence (**b**) were plotted against the rewiring probability. The delay was set to 1 ms between a neuron pair that is separated by 64 unit lengths, and was increased in proportion to the distance between presynaptic and postsynaptic neurons. The *inset* shows the scaling factors multiplied by the strength of AMPA synapses. They were identical to those used in Fig. 6

wiring was set to regular, small-world, or random connection patterns within a one-parameter family of the network topology.

Results of the present numerical simulations have shown that the regular and small-world neuronal networks formed intermittent clustered spikes, whereas such spike clusters rarely appeared in the random neuronal wiring. In the former two networks, recurrent connections densely interconnected nearby excitatory neurons, yielding relatively large clustering coefficients. The clustered neurons easily displayed a spatially localized excitation. Spike clusters should also be temporally localized, since short-term synaptic plasticity rapidly suppressed synaptic transmissions between the clustered neurons. The recovery of the synapses from the depression set the neuron clusters ready for another transient excitation. These above processes

repeated to produce a mixture of short and long ISIs, producing high Cv values in the present simulations.

The regular and small-world networks displayed large-amplitude membrane potential fluctuations that were presumably induced by correlated presynaptic spikes (Fig. 3(a)). Such correlated spike inputs have been proposed to be a likely source of the irregular firing of in vivo cortical neurons showing high Cv values (Stevens and Zador 1998). Our results indicate that the highly-clustered neuronal wiring in the regular and small-world networks produced highly irregular neuronal firing. Actually, the regular and small-world networks exhibited high probabilities of producing coincident spikes between adjacent neuron pairs (Fig. 5).

The existence of "short cuts" between distant nodes is a characteristic feature of the small-world network. A small fraction of such short-cut connections drastically reduces the average path lengths between an arbitrary node pair (Fig. 1). The short cut pathways allow the local neuronal activity to rapidly spread over the entire network, perhaps enhancing the global synchrony within the network activity (Netoff et al. 2004; Buzsáki et al. 2004). Our results obtained with a high conductance state of realistic neuron models were consistent with this naive expectation when the excitatory synapses were sufficiently strong (Figs. 5(d) and 6(b)). We, however, note that the small-world network topology produced no special effects on the network activity in other situations.

Somewhat unexpected results are the dependence of the spike coherence in the different wiring types on the synaptic strength. The spike coherence exhibited a large susceptibility to a subtle change in the synaptic strength in the randomly-wired network (Fig. 6(b)). It was previously proved that a randomly-connected network of integrate-and-fire neurons and delta-function synaptic couplings undergoes a phase transition from asynchronous to synchronous firing, when the excitatory synapses were gradually strengthened (Brunel 2000). Thus, the present results in the random network seem to be consistent with the above analytical results. By contrast, the phase-transition-like drastic changes in the spike synchrony disappeared in networks with small *p*, such as the regular and small-world networks (Fig. 6(b)). To our knowledge, these network-topology-dependent modulations of the spike coherence have not been known. In addition, the spike coherence was maximized for the network topology with an intermediate value of *p* (~0.1), only if the strength of recurrent excitatory synapses was within a certain range (see the result for the "×1.125" case in Fig. 6(b)). This property of the small-world network topology was previously suggested in a network of Hodgkin-Huxley neurons (Lago-Fernández et al. 2000). However, the present results have demonstrated that this advantage may not always be the case.

Increasing only the GABAergic conductance almost completely inhibited the network activity. It also reduced the spike variability and spike coherence since they reflect the transient increases in excitatory activities (Fig. 6). Increasing the AMPA conductance compensates for the above reductions in the spike variability and coherence, but not necessarily for the rate reduction. The changes in the spike coherence are consistent with the previous theoretical result that the fast-spiking interneurons coupled via GABAergic synapses exhibit asynchronous firing (Lewis and Rinzel 2003; Nomura et al. 2003). Although the inhibitory connections reduced the spike coherence and the network activity, the result in Fig. 6 suggested that characteristic behaviors of the spike statistics were essentially governed by excitatory synapses. The spike synchrony was maximized when both excitatory and inhibitory synaptic connections obey the small-world network topology (Fig. 7(b)). However, changing the topology of GABAergic synapses alone neither enhanced spike synchrony nor spike variability (Fig. 7(a,b)).

The degree of spike synchrony may crucially depend on the conduction delay (Traub et al. 1996; Ermentrout and Kopell 1998). To investigate the effect of the conduction delay, we introduced delays of about 1 ms into the synaptic transmissions of our model network that represents a local region of cortical networks. The conduction delays generated no qualitative changes in neither of the spike variability and spike coherence (Fig. 8).

The present model of local cortical networks is certainly over-simplified. Therefore, it is worth while comparing the present results with those of a more realistically modeled network. Dentate gyrus of the hippocampus exhibits structural reorganization during epileptogenesis. The reorganization undergoes two characteristic biological processes, the loss of hilar neurons and the sprouting of mossy fibers, in the dentate gyrus neuronal network. Recently, these changes were shown to enhance the overall small-world characteristic of the dentate gyrus network model, which consisted of several distinct neuron types (Dyhrfjeld-Johnsen et al. 2007). Moreover, the enhanced small-world characteristic resulted in hyperexcitability of the network activity. Interestingly, we may find a similar tendency in the results of the present simple network model: For instance, the average firing rate is increased in Fig. 6(c) as the network topology is changed from the small-world to a more regular type, as was the case in the dentate gyrus network model. We, however, note that the above changes in the small-world network topology occurred in a slightly different way in the two network models. In the present model, both clustering coefficient and the shortest mean path length increases toward the regular topology, whereas in the dentate gyrus model the latter is increased, but the former is decreased. This fact might suggest that the network excitability is more sensitive to the shortest mean path length. However, the network topologies have quite different description levels in the two models, and further careful inspections seem to be necessary to derive any conclusive statement.

In the present study, we applied noisy external input to neurons to enhance the irregular spontaneous activity. The existence of the external source of fluctuations limits the validity of our results demonstrating the significant influences of the network topology on the irregular neuronal firing. An interesting expansion of this study would be to feed the irregular output of each neuron back into the network in a recursive manner as the source of spontaneous activity, and to find a "fixed point" of this recursive map in the spike statistics. Such a study, however, requires a tremendous computational resource and remains open for further studies.

References

Achard, S., Salvador, R., Whitcher, B., Suckling, J., & Bullmore, E. (2006). A resilient, low-frequency, small-world human brain functional network with highly connected association cortical hubs. *Journal of Neuroscience*, *26*, 63–72.

Brunel, N. (2000). Dynamics of sparsely connected networks of excitatory and inhibitory spiking neurons. *Journal of Computational Neuroscience*, *8*, 183–208.

Buzsaki, G., Geisler, C., Henze, D. A., & Wang, X. J. (2004). Interneuron Diversity series: Circuit complexity and axon wiring economy of cortical interneurons. *Trends in Neurosciences*, *27*, 186–193.

Chow, C. C., & White, A. (1996). Spontaneous action potentials due to channel fluctuations. *Biophysical Journal*, *71*, 3013–3021.

Destexhe, A., Mainen, Z. F., & Sejnowski, T. J. (1998). Kinetic models of synaptic transmission. In C. Koch, & I. Segev (Eds.), *Methods in neural modeling* (pp. 1–25). Cambridge, MA: MIT.

Destexhe, A., & Paré, D. (1999). Impact of network activity on the integrative properties of neocortical pyramidal neurons in vivo. *Journal of Neurophysiology*, *81*, 1531–1547.

Destexhe, A., Rudolph, M., Fellous, J. M., & Sejnowski, T. J. (2001). Fluctuating synaptic conductances recreate in vivo-like activity in neocortical neurons. *Neuroscientist*, *107*, 13–24.

Dyhrfjeld-Johnsen, J., Santhakumar, V., Morgan, R. J., Huerta, R., Tsimring, L., Soltesz, I. (2007). Topological determinants of epileptogenesis in large-scale structural and functional models of the dentate gyrus derived from experimental data. *Journal of Neurophysiology, 97*, 1566–1587.

Erisir, A., Lau, D., Rudy, B., & Leonard, C. S. (1999). Function of specific K+ channels in sustained high-frequency firing of fast-spiking neocortical interneurons. *Journal of Neurophysiology*, *82*, 2476–2489.

Ermentrout, G. B., & Kopell, N. (1998). Fine structure of neural spiking and synchronization in the presence of conduction

delays. *Proceedings of the National Academy of Sciences of the United States of America*, 95, 1259–1264.

Foldy, C., Dyhrfjeld-Johnsen, J., & Soltesz, I. (2005). Structure of cortical microcircuit theory. *Journal of Physiology*, 562, 47–54.

Fukai, T. (2000). Neuronal communication within synchronous gamma oscillations. *NeuroReport*, 11, 3457–3460.

Gupta, A., Wang, Y., & Markram, H. (2000). Organizing principles for a diversity of GABAergic interneurons and synapses in the neocortex. *Science*, 287, 273–278.

Holmgren, C., Harkany, T., Svennenfors, B., & Zilberter, Y. (2003). Pyramidal cell communication within local networks in layer 2/3 of rat neocortex. *Journal of Physiology*, 551, 139–153.

Jahr, C. E., & Stevens, C. F. (1990). Voltage dependence of NMDA-activated macroscopic conductances predicted by single-channel kinetics. *Journal of Neuroscience*, 10, 3178–3182.

Kalisman, N., Siberberg, G., & Markram, H. (2005). The neocortical microcircuit as a tabula rasa. *Proceedings of the National Academy of Sciences of the United States of America*, 102, 880–885.

Koch, C. (1999). *Biophysics of computation*. New York: Oxford University Press.

Lago-Fernández, L. F., Huerta, R., Corbacho, F., & Sigüenza, J. A. (2000). Fast response and temporal coherent oscillations in small-world networks. *Physical Review Letters*, 84, 2758–2761.

Lewis, T. J., & Rinzel, J. (2003). Dynamics of spiking neurons connected by both inhibitory and electrical coupling. *Journal of Computational Neuroscience*, 14, 283–309.

Maass, W., Natschlager, T., & Markram, H. (2002). Real-time computing without stable states: A new framework for neural computation based on perturbations. *Neural Computation*, 14, 2531–2560.

Mainen, Z. F., & Sejnowski, T. J. (1995). Reliability of spike timing in neocortical neurons. *Science*, 268, 1503–1506.

Netoff, T. I., Clewley, R., Arno, S., Keck, T., & White, J. A. (2004). Epilepsy in small-world networks. *Journal of Neuroscience*, 24, 8075–8083.

Nomura, M., Fukai, T., & Aoyagi, T. (2003). Synchrony of fast-spiking interneurons interconnected by GABAergic and electrical synapses. *Neural Computation*, 15, 2179–2198.

Petersen, C. C. H. (2002). Short-term dynamics of synaptic transmission within the excitatory neuronal network of rat layer 4 barrel cortex. *Journal of Neurophysiology*, 87, 2904–2914.

Shadlen, M. N., & Newsome, W. T. (1998). The variable discharge of cortical neurons: Implications for connectivity, computation, and information coding. *Journal of Neuroscience*, 18, 3870–3896.

Shinomoto, S., Miyazaki, Y., Tamura, H., & Fujita, I. (2005). Regional and laminar differences in in vivo firing patterns of primate cortical neurons. *Journal of Neurophysiology*, 94, 567–575.

Softky, W. R., & Koch, C. (1993). The high irregular firing of cortical cells is inconsistent with temporal integration of random EPSPs. *Journal of Neuroscience*, 13, 334–350.

Song, S., Sjöström, P. J., Reigl, M., Nelson, S., & Chklovskii, D. B. (2005). Highly nonrandom features of synaptic connectivity in local cortical circuits. *PLoS Biology*, 3, e68.

Sporns, O., & Zwi, J. D. (2004). The small world of the cerebral cortex. *Neuroinformatics*, 2, 145–162.

Stepanyants, A., Tamás, G., & Chklovskii, D. B. (2004). Class-specific features of neuronal wiring. *Neuron*, 43, 251–259.

Stevens, C. F., & Zador, A. M. (1998). Input synchrony and the irregular firing of cortical neurons. *Nature Neuroscience*, 1, 210–217.

Traub, R., Whittington, M., Stanford, M., & Jefferys, J. (1996). A mechanism for generation of long-range synchronous fast oscillations in the cortex. *Nature*, 383, 621–624.

Tsodyks, M., & Markram, H. (1997). The neural code between neocortical pyramidal neurons depends on neurotransmitter release probability. *Proceedings of the National Academy of Sciences of the United States of America*, 94, 710–723.

Wang, X. J., & Buzsáki, G. (1996). Gamma oscillation by synaptic inhibition in a hippocampal interneuron network model. *Journal of Neuroscience*, 16, 6402–6413.

Watts, D. J., & Strogatz, S. H. (1998). Collective dynamics of 'small-world' networks. *Nature*, 393, 440–442.

Wolfart, J., Debay, D., Le Masson, G., Destexhe, A., & Bal, T. (2005). Synaptic background activity controls spike transfer from thalamus to cortex. *Nature Neuroscience*, 8, 1760–1767.

Yoshimura, Y., & Callaway, E. M. (2005). Fine-scale specificity of cortical networks depends on inhibitory cell type and connectivity. *Nature Neuroscience*, 8, 1552–1559.

Yoshimura, Y., Dantzker, J. L. M., & Callaway, E. M. (2005). Excitatory cortical neurons from fine-scale functional networks. *Nature*, 433, 868–873.